Nuclear Materials and Energy 36 (2023) 101497

Contents lists available at ScienceDirect

Nuclear Materials and Energy

journal homepage: www.elsevier.com/locate/nme

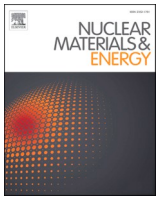

Comparative analysis of low cycle fatigue behavior of pre-corroded standard and sub-sized EUROFER97 specimens exposed to ceramic breeder environment

E. Gaisina *, R. Gaisin, J. Leys, R. Knitter, J. Aktaa, M. Walter

Karlsruhe Institute of Technology (KIT), Institute for Applied Materials, Hermann-von-Helmholtz-Platz 1, 76344 Eggenstein-Leopoldshafen, Germany

ARTICLE INFO

Keywords:
EUROFER97
Ceramic breeder
Corrosion
Fatigue

ABSTRACT

In the helium-cooled pebble bed blanket concept of DEMO, the reduced activation ferritic-martensitic steel EUROFER97 will be in direct contact with lithium ceramic pebbles and undergo cyclic thermomechanical loading during operation. This study compares the impact of pre-corrosion for 64 days, simulating working conditions of EUROFER97, on the microstructure and low cycle fatigue properties of full-sized standard and sub-sized specimens. In both cases, the pre-corrosion process leads to the formation of three layers with a combined thickness of approximately 17 μm. Standard specimens (Ø8.8 mm) exhibit a notable decrease in fatigue life after pre-corrosion, though not as severe as the sub-sized specimens (Ø2 mm). At a 0.6 % strain range, pre-corroded standard and sub-sized specimens experience a reduction in fatigue life by 35 % and 60 %, respectively. Microstructural studies reveal, that surface micro-cracks, commonly observed after exposure at contact zones with lithium ceramic pebbles, accelerate the evolution of surface damage during cycling and often act as initiation sites for fatigue crack. Potential factors contributing to the observed difference in fatigue life based on specimen size are discussed. The estimated maximum allowable deformation range of EUROFER97 components, without considering creep and neutron irradiation effects, is determined to 0.25 %.

1. Introduction

The reduced activation ferritic-martensitic (RAFM) steel EUROFER97 is planned to be used as a structural material in the helium-cooled pebble bed (HCPB) blanket concept of the DEMO fusion reactor [1–3]. In this concept, EUROFER97 is chosen as the material for tubes in fuel-breeder pins, which are filled with a ceramic breeder material consisting of 70 mol.% Li_4SiO_4 + 30 mol.% Li_2TiO_3 pebbles [4]. The primary objective of this configuration is to generate tritium under neutron irradiation, which acts as fuel for the fusion reaction.

The interaction between the lithium ceramic pebbles and the inner surface of the EUROFER97 components is of utmost importance, given the complex operational conditions they undergo. These components experience alternating tension and compression due to the cyclic heating and cooling process of the DEMO reactor. Furthermore, the EUROFER97 components are exposed to helium flow from the outside and purged with a mixture of He and 0.1 vol% H_2 from the inside, which may contain impurities and contribute to corrosion. All these factors must be carefully considered, especially given the conditions of high temperatures up to 550 °C and an intense flux of high-energy neutrons.

Our previous studies have conducted experiments to partially simulate the operating conditions of EUROFER97 in the HCPB blanket [5,6]. These experiments involved the use of sub-sized specimens with a gauge length diameter of 2 mm. The sub-sized specimens underwent pre-corrosion by exposing them to lithium ceramic pebbles in a purge gas atmosphere at 550 °C for a duration of 8–128 days. Following the exposure, low-cycle fatigue (LCF) tests were performed on the pre-corroded specimens. The results revealed a significant reduction in the fatigue lifetime as the exposure duration increased up to 32 days. However, beyond an exposure duration of 64 days, there was no further decrease in the lifetime, due to the cessation of the growth of the corrosion layer thickness after the same exposure time [6]. Based on these findings, it was determined that the duration of exposure could be limited to 64 days since longer exposure had minimal effects on the corrosion layer thickness and the fatigue lifetime in LCF tests.

The use of sub-sized samples allowed for a large number of tests (over 100) to be conducted within a reasonable timeframe, enabling the identification of general trends. However, for more reliable fatigue test

* Corresponding author.
E-mail address: elvina.gaisina@kit.edu (E. Gaisina).

https://doi.org/10.1016/j.nme.2023.101497
Received 10 July 2023; Received in revised form 15 August 2023; Accepted 29 August 2023
Available online 29 August 2023

results, it is necessary to repeat these tests on full-sized standard specimens with a larger gauge length diameter of 8.8 mm. It remains unknown whether testing standard pre-corroded specimens will yield similar deterioration in fatigue life as observed in the sub-sized specimens. Furthermore, it is uncertain whether pre-corrosion will result in the formation of a similar corrosion layer. This paper aims to discuss the causes of deterioration in fatigue life and explore potential differences in the fatigue behavior between standard and sub-sized specimens. Additionally, an assessment of the maximum allowable deformations of EUROFER97 will be conducted based on the results of this study.

2. Experimental details

RAFM steel EUROFER97 batch 2 was used as the material for the study. The steel, with a nominal composition of Fe-8.5Cr-1.1 W-0.2Mn-0.15 V-0.12Ta-0.1C (wt.%), was heat-treated (960 °C for 1.5 h, oil quenching + 750 °C for 4 h, air cooling) prior to the experiments. This heat-treated state is referred to as-received in the paper. For the low cycle fatigue (LCF) investigations, standard specimens were prepared with a nominal diameter of 8.8 mm and a gauge length of 23 mm. Additionally, data from previous studies on sub-sized specimens [5,6] were included for comparison purposes. The working part of these specimens had a nominal diameter of 2 mm and a gauge length of 7.6 mm.

Pre-corrosion experiments were conducted in pressurized furnaces at 550 °C using a purge gas flow atmosphere. The purge gas, consisting of He and 0.1 vol% H_2, was maintained at a flow rate of 1200 ml/min at a pressure of 1200 mbar. The amount of gas impurities, particularly oxygen and water, was measured as 0.14–0.24 vol% and 0.005–0.08 vol%, respectively. The oxygen content remained approximately the same at both the inlet and outlet, showing no significant changes over time, while the water content consistently exhibited higher levels at the outlet in comparison to the inlet, gradually decreasing from a maximum value at outlet of 0.08 vol% after 5 days to 0.02 vol% after 128 days of the experiment. The EUROFER97 specimens were placed in open ceramic containers and completely covered with lithium ceramic pebbles. The pebbles used in the experiment were spherical in shape and had a size ranging from 250 to 1250 μm. These pebbles were composed of a mixture of 70 mol.% lithium orthosilicate (Li_4SiO_4) and 30 mol.% lithium metatitanate (Li_2TiO_3) [6]. The exposure time for the standard specimens was 64 days. Henceforth, the conditions designed to simulate the EUROFER97 operating environment in the blanket will be referred as the "ceramic breeder environment" for the sake of simplicity.

Strain-controlled LCF tests were performed in air at 550 °C, applying various strain ranges: 0.4 %, 0.6 %, 0.8 %, 1 %, 1.2 %, and 1.6 %. The tests utilized a strain rate of 3×10^{-3} s^{-1} and a fully-reversed triangular waveform ($R = -1$). The tests were carried out according to the ASTM A. E2714-13 standard [7]. To analyze the microstructural features of the specimens, scanning electron microscopy (SEM) combined with energy dispersive X-ray spectroscopy (EDS) was employed. Surface and cross-sections of the samples were examined using this characterization technique.

3. Results and discussion

3.1. Effect on the microstructure

Fig. 1 depicts the appearance of standard LCF specimens in the as-received state and after exposure to the ceramic breeder environment for 64 days. After the exposure, the specimens displayed a bluish surface color resembling that of the sub-sized specimens shown previously in [6]. The contact zones with the lithium ceramic pebbles are clearly visible to the naked eye, revealing a portion of the pebbles that adhered to the surface during exposure (Fig. 1). These pebbles are easily dislodged from the surface and were manually removed before conducting the fatigue test. The distance between the centers of contact zones represents the average diameter of the pebbles.

Fig. 1. Standard (Ø8.8 mm) LCF specimens made of EUROFER97 in the as-received state (top) and after exposure to the ceramic breeder environment for 64 days (bottom).

On the SEM micrographs (Fig. 2a) prominent imprints, resulting from contact with lithium ceramic pebbles, are the main feature of the surface. The diameter of the imprints corresponds approximately to the size of the pebbles. Notably, at the center of almost each imprint, a pit is consistently present, providing insight into the internal structure of the corrosion layer (Fig. 2b). Moreover, micro-cracks tend to propagate from the central region of the imprints, extending up to a distance of approximately 100–200 μm. Additionally, hillocks are observed at the periphery of the imprints (Fig. 2c). These hillocks consist of ferrite formations that develop on the surface of iron oxide due to its reduction with hydrogen as also shown in [6,8,9]. It is worth mentioning that the hillocks can exhibit heterogeneous cross-sections and may contain iron oxide crystals in the core (Fig. 2d).

Fig. 3 presents the SEM surface microstructure of a EUROFER97 specimen after exposure to the ceramic breeder environment, along with corresponding EDS maps. The analysis focused on an imprint with a peeled surface, revealing an internal corrosion layer enriched in chromium and oxygen as shown in Fig. 3c-d. Surrounding the imprints, a layer of pure iron with hillocks can be observed on the surface. These surface characteristics align with previous findings on sub-sized samples and microstructural investigations [6], indicating the consistency and reproducibility of the results.

In the cross-sectional view, the corrosion layer can be divided into three distinct layers labeled as A, B, and C in Fig. 4. The outer layer A comprises a combination of pure iron (light gray phase) and iron-rich oxide (dark phase). The intermediate layer B consists of chromium-enriched oxides. As was shown in the separate TEM study [10], this layer is formed by lithium containing spinel. The inner corrosion layer is EUROFER97 with chromium-enriched oxides (spinel) particles along grain/laths boundaries. The thickness of the corrosion layer in the standard specimen, exposed to the ceramic breeder environment for 64 days, ranged from 15 to 20 μm, with an average thickness of 17 μm. This thickness closely corresponds to the corrosion layer observed in sub-sized specimens after the same exposure. Hence, the exposure of the standard specimen to the ceramic breeder environment led to the formation of a corrosion layer with almost the same structure and thickness as observed in the case of sub-sized specimens [6].

3.2. Effect on the fatigue life

Fig. 5 presents diagrams of tensile peak stress versus number of cycles for different total strain ranges, including two curves for both standard and sub-sized specimens in the as-received state and after exposure to the ceramic breeder environment for 64 days. Fatigue tests were conducted under the same conditions in air and were accompanied by minor surface corrosion. It was decided not to take into account the

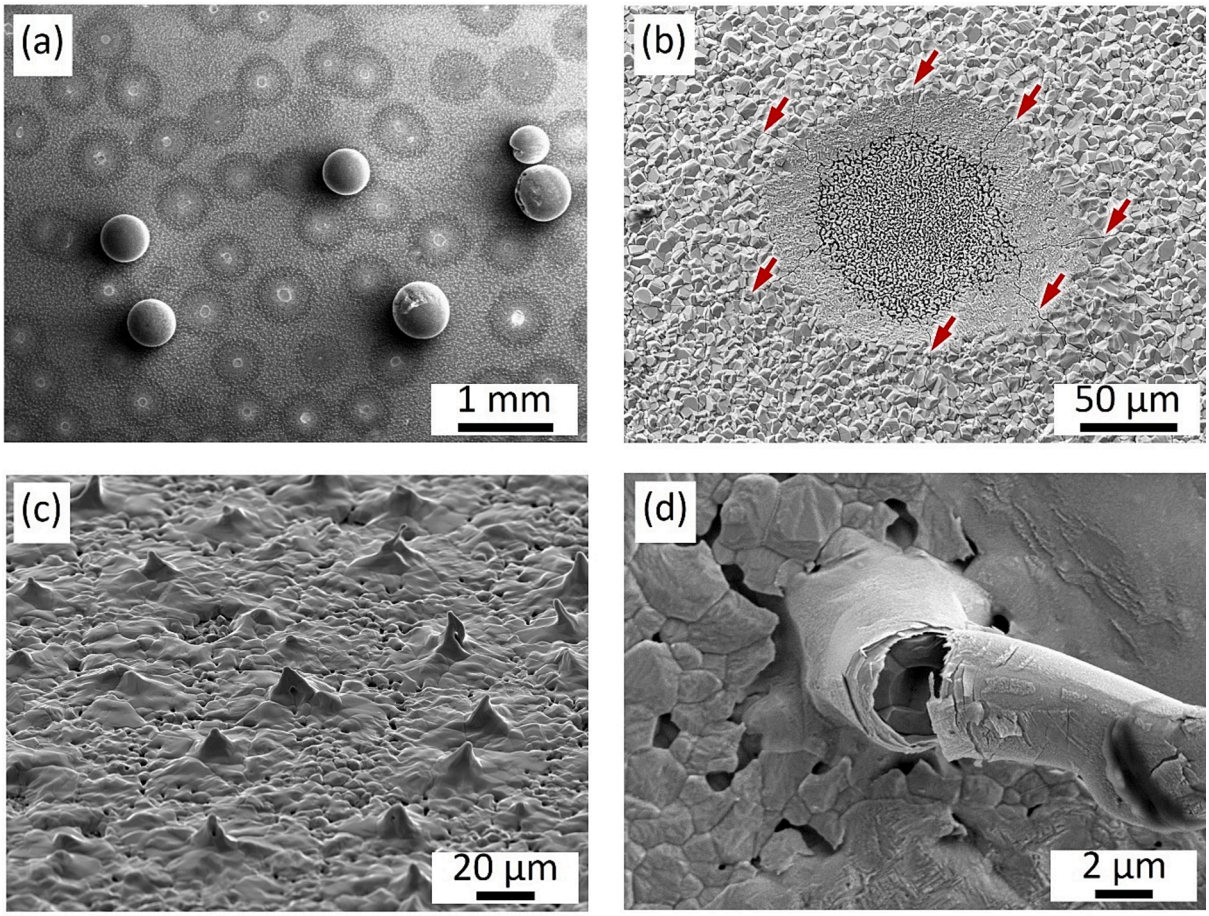

Fig. 2. Microstructure of the surface after pre-corrosion: (a) imprints together with adherent pebbles, (b) imprint with cracks indicated by red arrows, (c) ferrite hillocks surrounding the imprints on the surface (45° view), (d) internal structure of one of the hillocks.

effect of this short-term corrosion, but to isolate and identify the effect of pre-corrosion. For all samples, fatigue softening behavior typical of EUROFER97 is observed. The first stage for all four curves (at all corresponding total strain ranges) practically coincides, but the duration of the linear second stage differs, resulting in the as-received standard specimens (blue curves, $N_f = 5100$ cycles for $\Delta\varepsilon_{tot} = 0.6$ %) enduring a greater number of cycles to failure than the as-received sub-sized specimens (red curves, $N_f = 3100$ cycles for $\Delta\varepsilon_{tot} = 0.6$ %) under the same test conditions.

The pre-corroded standard specimens (light blue curves, $N_f = 3250$ cycles for $\Delta\varepsilon_{tot} = 0.6$ %) showed a longer fatigue life compared to the pre-corroded sub-sized specimens (pink curves, $N_f = 1150$ cycles for $\Delta\varepsilon_{tot} = 0.6$ %) and even a slightly longer lifetime compared to the as-received sub-sized specimens (red curves). However, the undoubted decrease in fatigue lifetime associated with exposure to the ceramic breeder environment, is observed for standard specimens. The observed effects remain for all tested full strain ranges, and the scatter in life values is greater for larger values of the full strain range, when loads become high, and the effect of pre-corrosion attack can decrease.

The Wöhler diagram for the standard and sub-sized specimens in both as-received and pre-corroded conditions (64 days in the ceramic breeder environment) is presented in Fig. 6. Evidently, the standard specimens endured more cycles to failure compared to the corresponding sub-sized specimens. Exposure to the ceramic breeder environment for 64 days has a pronounced effect of deteriorating fatigue life for both sub-sized and standard specimens. For sub-sized specimens, the degradation in fatigue life is 60 %, 40 %, and 35 % for total strain ranges of 0.6 %, 1 %, and 1.6 %, respectively. However, for standard specimens, the effect was less dramatic, with an average degradation of 35 %, 10 %, and 30 % for the same total strain ranges. The greatest deterioration effect was observed for the total strain range of 0.6 % for both sub-sized and standard specimens. As the total strain range increases, the effect decreases and can be covered by data scattering. As the tests for standard specimens were carried out in accordance with the ASTM standard [7], the fatigue life values obtained for them are more reliable.

3.3. Factors of fatigue life deterioration

One of the evident factors contributing to the premature failure of EUROFER97 specimens exposed to the ceramic breeder environment is the presence of pre-existing cracks on the EUROFER97 surface even prior to LCF testing. As illustrated in Fig. 2b, such exposure leads to surface cracking from almost each imprint. The cracks propagate radially from the center of the imprint and deviate in different directions depending on the crystals orientation. This suggests that the cracks were formed after exposure, most likely during the cooling stage of the samples. If the cracks were pre-existing, the crystals could grow and heal the crack during exposure so that the cracks would not be visible on the surface.

After exposure, the specimens were cooled from 550 °C to room temperature at a relatively slow rate of approximately 32 K/h. However, the corrosion layer can experience tensile stresses during cooling independently to the cooling rate as a result of the difference in thermal expansion coefficients. Stresses arise due to the fact that a massive substrate in the form of EUROFER97 specimen shrinks when cooled, regardless of the presence of a thin corrosion film on the surface. In this case, the corrosion layer, being adhered to EUROFER97, will have to shrink by the same amount as the substrate. The thermal expansion

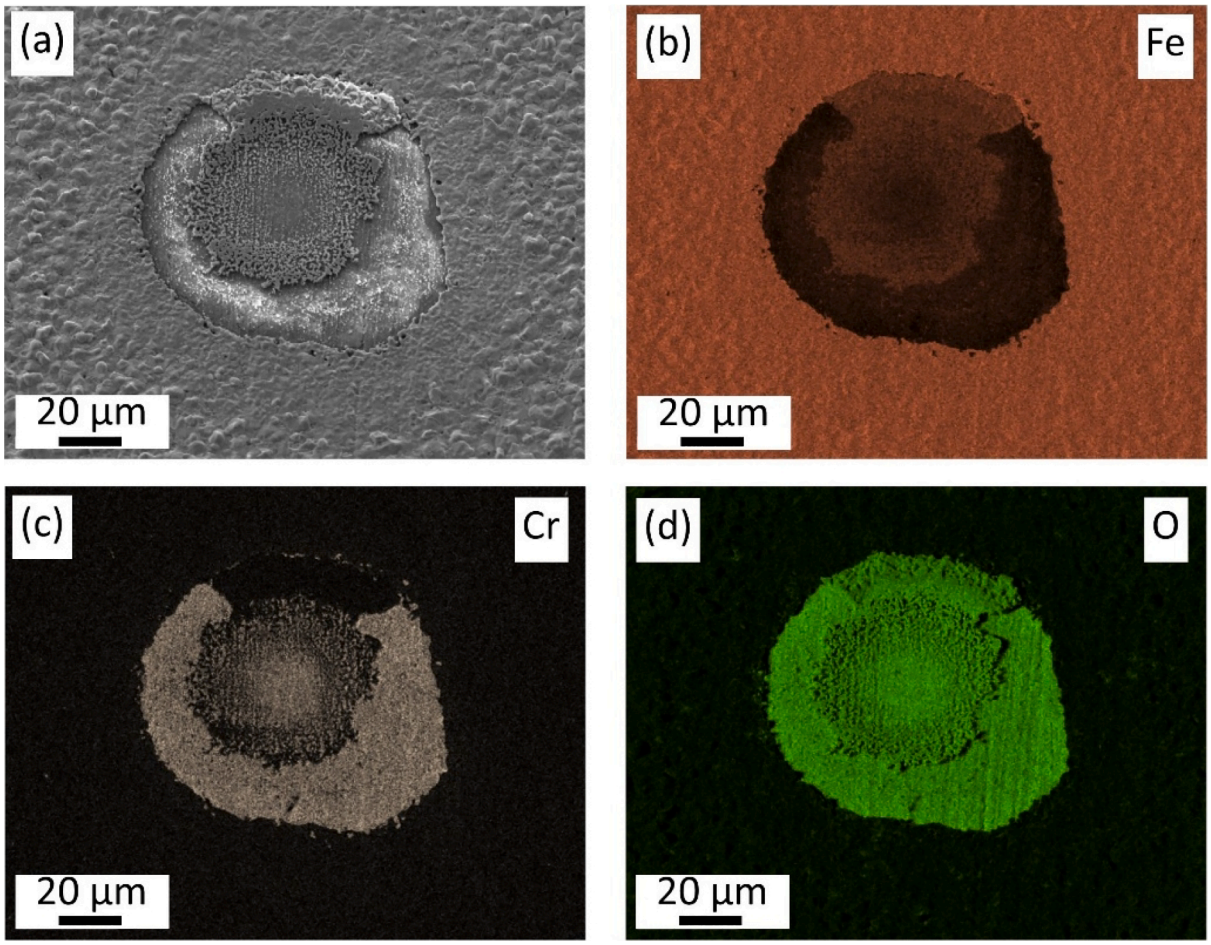

Fig. 3. (a) Microstructure and (b-d) corresponding elemental EDS maps of a surface of EUROFER97 specimen exposed to the ceramic breeder environment for 64 days: (b) iron, (c) chromium, (d) oxygen.

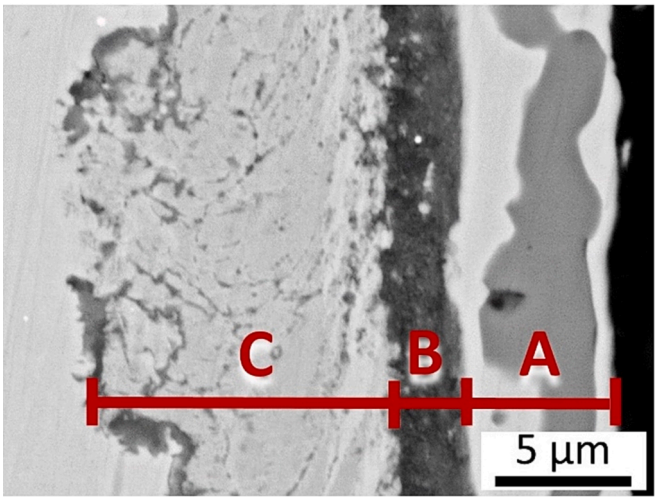

Fig. 4. SEM microstructure of a cross section of a standard EUROFER97 sample exposed to the ceramic breeder environment for 64 days. Three distinct corrosion layers are identified and labeled with capital letters.

coefficients of iron oxide and chromium-rich oxide are likely differ to that of EUROFER97, causing the surface layer to be under tension/compression. The imprints, acting as pits, can concentrate these stresses and lead to cracking.

Imprints of lithium ceramic pebbles not only can serve as sites of crack initiation during the cooling of specimens after exposure, but what is more important, also during the fatigue tests. These imprints, along with the pre-existing cracks, can act as significant stress concentrators during the tests. Point defects in the form of pits pose a greater risk for crack initiation compared to general corrosion, which spreads uniformly over the surface. These pits or cracks concentrate stress and act as notches, making crack initiation more likely.

Fig. 7 displays video macro shots of LCF testing performed on one of the standard EUROFER97 specimens following a 64-day exposure to the ceramic breeder environment with a total strain range of 1.6 %. During the initial cycles up to approximately $0.75N_f$, the predominant behavior observed is the formation and propagation of micro-cracks (smaller than 1000 μm). It is only at around 300 cycles that visible cracks become apparent (as shown in Fig. 7b). The red circles in the figure indicate the specific imprints through which the crack propagates, while other imprints do not exhibit such cracking behavior. As testing progresses and reaches approximately 340 cycles, a fatigue crack develops along a part of the imprints previously indicated by red circles. Other cracks cease opening on the imprints due to the onset of strain localization (Fig. 7c). While the number of cycles to failure N_f for this particular specimen was calculated to be 388, the testing continued up to 410 cycles. At this point, the fatigue crack opened entirely, resulting in the fracture of the specimen (Fig. 7d). These observations indicate that the cracks present on the imprints after exposure represent pre-existing defects that can propagate further during fatigue testing, leading to the development of a fatigue crack.

Fig. 8 shows typical EUROFER97 specimens after the exposure to the ceramic breeder environment for 64 days and subsequent LCF tests. In

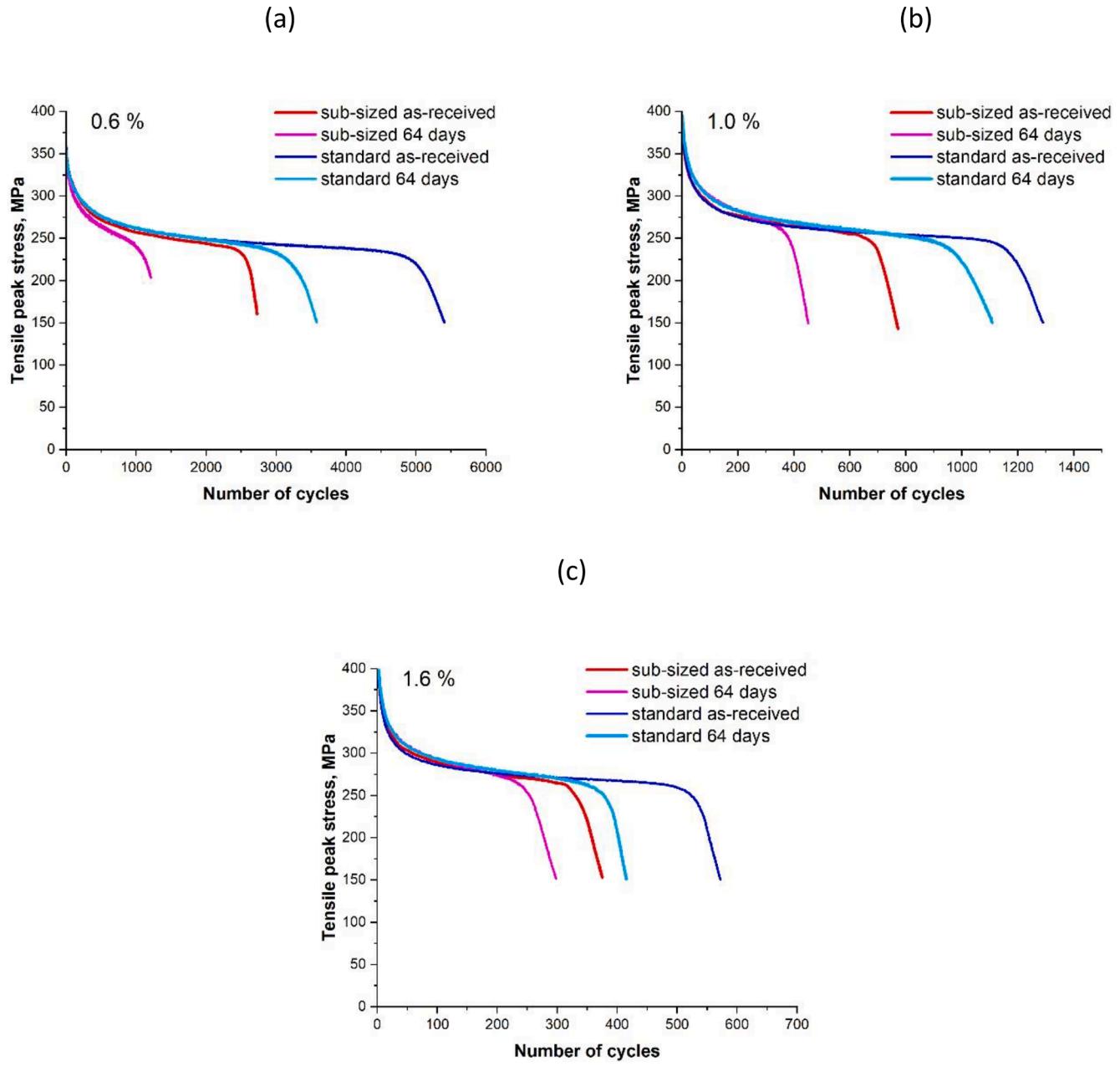

Fig. 5. Typical tensile peak stress versus the number of cycles for sub-sized and standard specimens tested at a total strain range of (a) 0.6 %, (b) 1 %, and (c) 1.6 %.

the case of a sub-sized specimen with a 2 mm diameter (Fig. 8a), only a few imprints can be seen close to the fatigue crack. It is evident that the fatigue crack runs along the diameter of at least one of the imprints. Additionally, the imprint, which is somewhat distant from the fracture zone, also cracked in diameter. On the other hand, in the case of a standard specimen with an 8.8 mm diameter (Fig. 8b), there are 4.2 times more imprints per cross-section in terms of geometry. In this case, it can be observed that the crack predominantly passes through imprints, but not as clearly as in the case of sub-sized specimens. Fig. 8c and 8d show specimens that underwent LCF testing and were cut along their length to examine how deeply cracks propagate from imprints. It is clear from the figures that cracks can penetrate deep into the sample, sometimes several hundred microns, even far from the fracture zone. These observations suggest that the imprints serve as sites for fatigue crack initiation and that the cracks observed on the surface, passing through or starting on imprints, are not limited to surface cracks passing through a relatively brittle corrosion layer.

The study of EUROFER97 specimens after exposure to the ceramic breeder environment and LCF tests showed that the presence of pre-existing micro-cracks, which arise during cooling due to the difference in coefficient of thermal expansion, and imprints themselves have a significant effect on fatigue life. These micro-cracks on imprints serve as fatigue crack initiation sites and facilitate their growth. The number of cycles to failure for pre-corroded specimens decreases due to the presence of such cracks, since no time is required for the initiation of surface damage in form of micro-cracks. Fatigue cracks were observed to grow predominantly along the pre-existing small cracks on imprints.

3.4. *Size effect*

As illustrated in Figs. 5 and 6 standard specimens exhibited greater fatigue life in comparison to sub-sized specimens under similar conditions, but the reasons for this behavior are unclear. Given that the number of cycles required for fracture is partly affected by the nature of

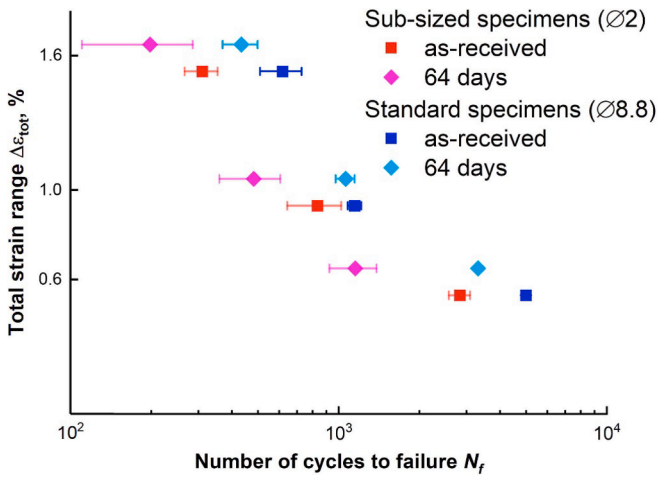

Fig. 6. Results of the LCF tests of EUROFER97 sub-sized and standard specimens in as-received and pre-corroded (64 days) conditions. The specimens were tested at 550 °C at three different total strain ranges of 0.6, 1, and 1.6 %. Vertical offset within a strain range is used to avoid data overlap.

the fracture and the development of fatigue crack, it is reasonable to explore the fracture surfaces of sub-sized and standard specimens. Fig. 9 presents the fracture surface of a pre-corroded sub-sized specimen, as well as a panoramic photo (owing to its significantly larger size) of a pre-corroded standard specimen after LCF testing with a total strain range of 1.6 %. Notably, the fractography exhibits clear evidence of crack propagation in each cycle, known as striation, despite surface oxidation (tests were conducted at 550 °C in air). The crack growth marks often coincide at the beginning of the test, likely due to small crack growth and surface oxidation.

To gain a deeper understanding of the fracture mechanical differences between standard and sub-sized specimens, the crack propagation rate was measured for specimens where possible. For each cycle, starting from the last one, the crack depth was measured as a distance from the initiation point (Fig. 10). Note that the last test cycle is not equivalent to the N_f cycle, i.e., the number of cycles to failure. The fatigue crack depths for both standard and sub-sized specimens were approximately half the diameter 4.4 mm and 1 mm, respectively, before final failure. At the end of the test, the crack depth increments were approximately 100 μm and 25 μm for the standard and sub-sized specimens, respectively. In general, the crack growth pattern for standard and sub-sized specimens is similar, with rapid crack growth occurring for the standard specimen after approximately 300 cycles, and for the sub-sized specimen, after about 100 cycles. Under the assumption that the fracture initiates from a crack with depth in the range of micrometers, the measured data can be fitted with dashed curves shown in Fig. 10.

It should be noted that the accelerated development of surface damage in sub-sized specimens will contribute to the reduction in the number of cycles to failure compared to standard specimens. Future work will involve interrupted fatigue tests with measurements of crack length and depth using focused ion beam techniques, while the current study primarily focuses on fractography analysis. Furthermore, it is important to acknowledge that the growth of fatigue cracks in cylindrical specimens is affected by the orientation of the crack related to the position of the extensometer at strain controlled conditions and that fatigue cracks do not necessarily propagate strictly perpendicular to the applied load. To obtain more precise measurements of crack depth, compact tension specimens (CT) would be required for specific testing in accordance with standards.

The fatigue crack growth rate da/dN is dependent on the stress intensity factor range ΔK, following the Paris-Erdogan law:

$$\frac{da}{dN} = C \bullet \Delta K^m \tag{1}$$

where C and m are material constants, and ΔK is the stress intensity factor range. The stress intensity factor range in its turn can be calculated as:

$$\Delta K = F_n \bullet \Delta\sigma \bullet \sqrt{\pi \bullet a} \tag{2}$$

where F_n is a dimensionless geometric factor that is dependent on the geometry of the crack, $\Delta\sigma$ is the applied stress range, and a is the crack depth.

The geometric factor is a critical component in the above equations as it takes into account the differing geometric dimensions of the sub-sized and standard specimens. In the case of a crack in cylindrical specimens, the geometric factor can be calculated using the following

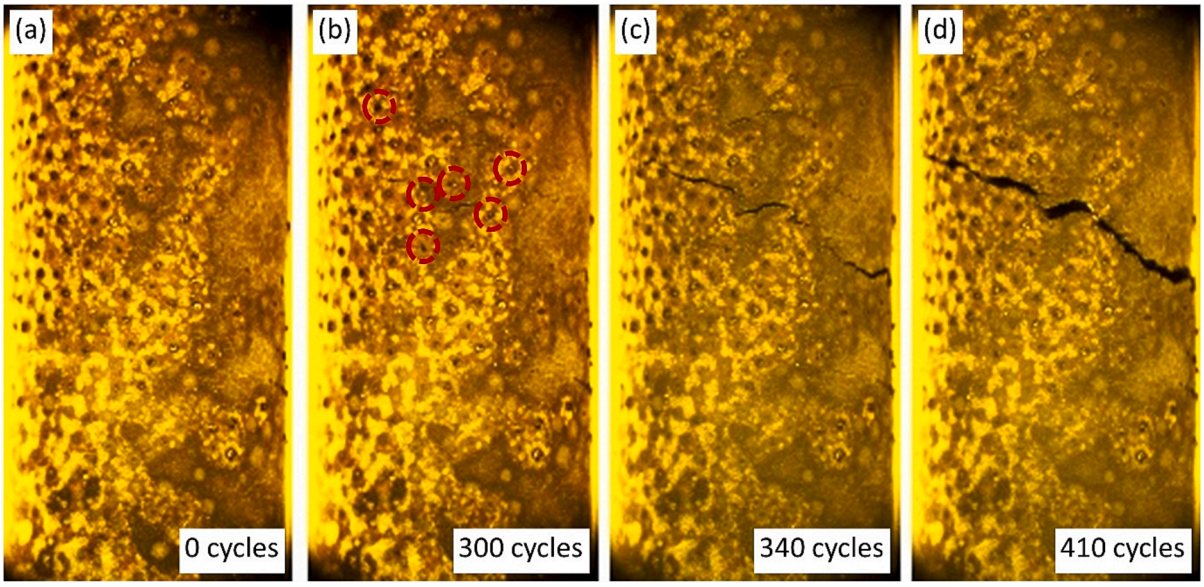

Fig. 7. Video macro shots of LCF test of a pre-corroded standard EUROFER97 specimen: (a) the beginning of the test, (b) after 300 cycles, (c) after 340 cycles, and (d) after 410 cycles. The total strain range was 1.6 %, and the number of cycles to failure is 388 cycles. The diameter of the specimen is 8.8 mm. In (b), the red circles indicate the imprints on which cracks opened during the tension.

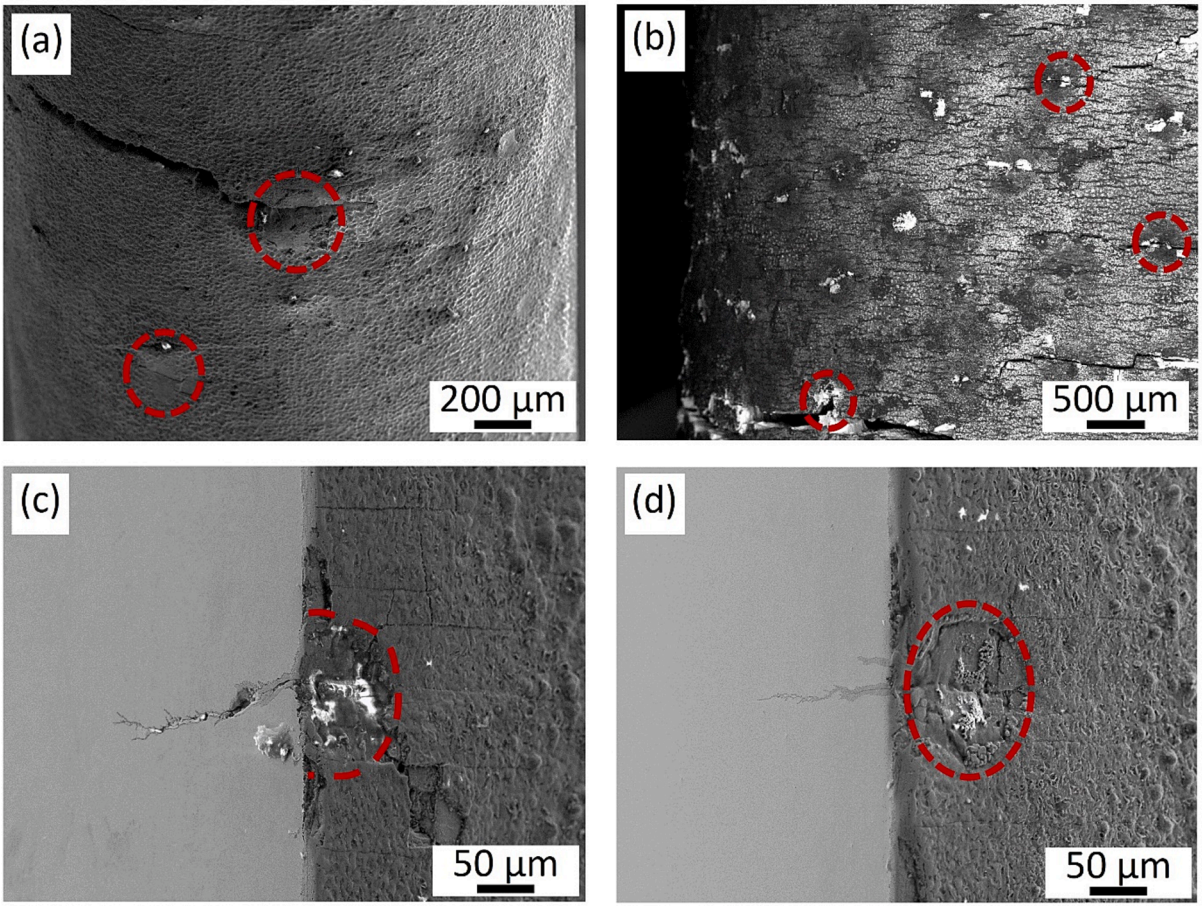

Fig. 8. Propagation of pre-existing cracks on imprints following LCF testing of EUROFER97 specimens exposed to the ceramic breeder environment: (a,b) surface, (c, d) longitudinal section; (a,c) sub-sized and (b,d) standard specimens. Imprints are indicated by red circles.

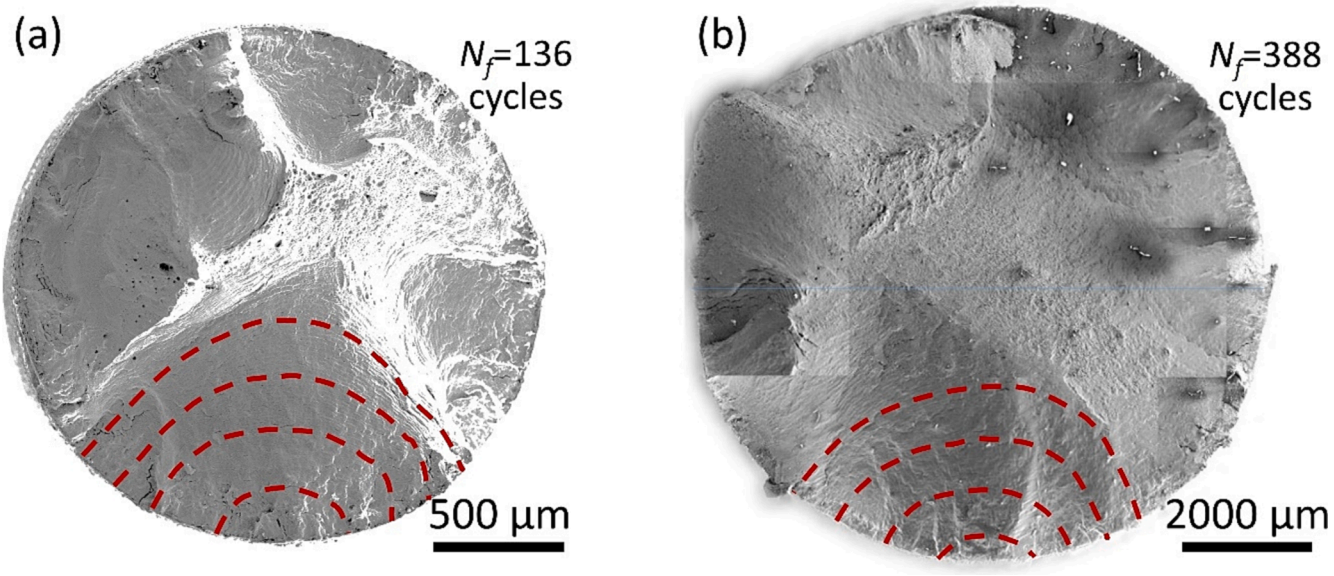

Fig. 9. The fracture surface of specimens after LCF test: (a) sub-sized specimen of Ø2 mm with $N_f = 136$ cycles to failure, (b) standard specimen of Ø8.8 mm with $N_f = 388$ cycles to failure. Total strain range 1.6 %. The red dashed lines indicate the propagation path of a fatigue crack.

equation [11–13].

$$F_n = 0.92 \bullet \frac{2}{\pi} \bullet sec\beta \bullet \sqrt{\frac{tan\beta}{\beta}} \bullet (0.752 + 1.286 \bullet \beta + 0.37 \bullet Y^3) \quad (3)$$

where $Y = 1 - sin\beta$ and $\beta = \frac{\pi}{2} \bullet \frac{a}{D}$. In the last equation, D is the diameter of the specimen, so the geometric factor depends on it in a complex way.

The dependence of the geometric factor F_n on the crack depth a, calculated using equation (3), is presented in Fig. 11. Notably, the

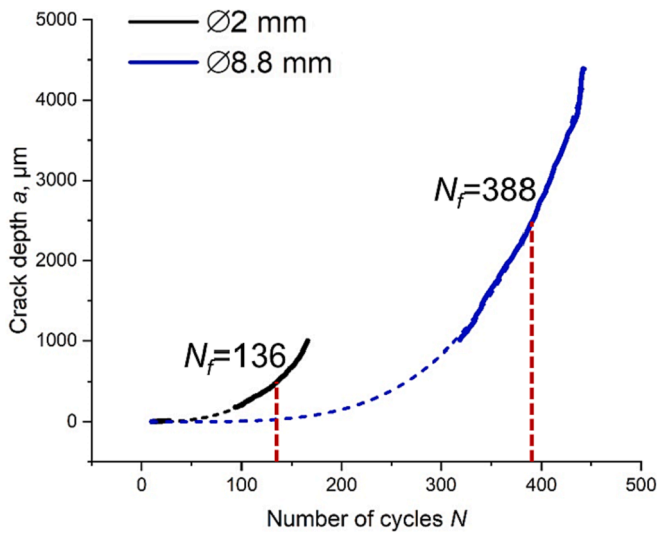

Fig. 10. The fatigue crack depth in the pre-corroded sub-sized (black) and standard (blue) specimens as a function of the number of cycles during LCF testing. The measured crack depth based on fractography is indicated by solid lines, while the corresponding fitted curves are represented by dashed lines.

geometric factor increases more gradually for the standard specimen compared to the sub-sized specimen. For example, for a crack depth of 0.5 mm, the geometric factor is 0.675 and 0.875 for the standard and sub-sized specimen, respectively. For a crack depth of 1 mm, the corresponding values are 0.711 and 1.655. Thus, it is evident that cracks of the same depth result in significantly different geometric factors for specimens of different sizes. In other words, a specimen with a larger diameter is less sensitive to a crack of the same size as in a sub-sized specimen, and therefore can withstand a greater number of cycles. This may explain partly the greater fatigue life of standard specimens as shown in Figs. 5 and 6.

3.5. Estimation of lifetime of components

The knowledge gained in the course of the work showed a considerable reduction in the fatigue life of EUROFER97 specimens exposed to the ceramic breeder environment for an extended period of time.

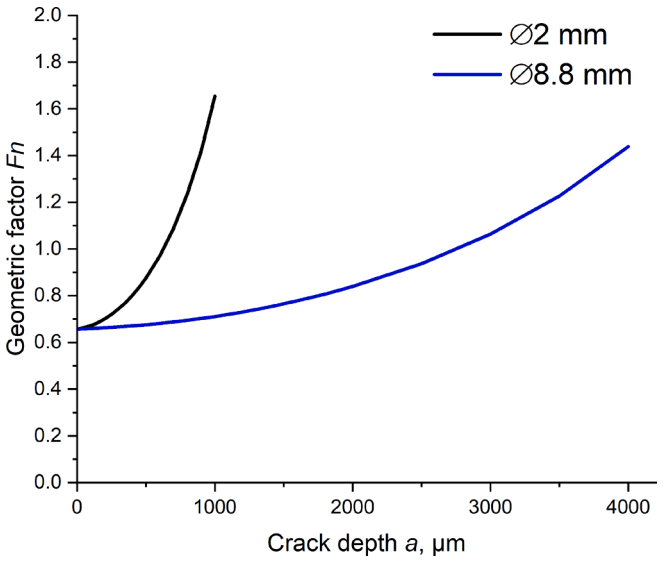

Fig. 11. The calculated value of the geometric factor depending on the depth of the crack in the sub-sized and standard specimens.

However, it is important to acknowledge that the experiments only partially mimic the operational conditions of EUROFER97 components in the DEMO breeder blanket. Under intense irradiation with high-energy neutrons and a maximum dose of up to 20 dpa by the end of the first phase [14,15], it is probable that the fatigue properties will deteriorate even further. The real interaction between EUROFER97 and the Li-ceramic pebble bed in a purge gas atmosphere, under variable tension and compression, remains unclear, since simultaneous corrosion fatigue will develop instead of pre-corrosion fatigue studied in the work. Another critical factor, which was not taken into account, is the creep of EUROFER97 tubes that can occur after a period of rapid heating during two hours of full power operation at high temperature. This, in turn, will exacerbate the decrease in fatigue life.

Nevertheless, to determine the permissible operating conditions of EUROFER97 components in contact with Li-ceramic pebbles in the breeder blanket, a fundamental approach was adopted in this study. The Wöhler diagram was used to demonstrate how many cycles to failure the specimen can withstand, depending on the total strain range experienced. Additional tests were conducted on standard EUROFER97 specimens exposed to the ceramic breeder environment for 64 days, using total strain ranges of 0.4 %, 0.8 %, and 1.2 %, to increase the number of data points.

Fig. 12 displays a Wöhler diagram including additional test results for other total strain ranges for standard as-received EUROFER97 specimens. A curve was generated for six data points using automated fitting to minimize the sum of squared deviations. The total strain range follows the equation $\Delta\varepsilon_{tot} = 0.00382 + 3.74663 \cdot N^{-0.89846}$, where N represents the number of cycles to failure and the total strain range is presented as a fraction (not in percentage).

With the available data and the fitting curve, it is possible to estimate the allowable maximum total strain range for a known number of cycles that a component undergoes. One of the approaches to achieve this is the use of ASME Code Case N-47, which provides guidelines for the evaluation of LCF in nuclear power plant components. This code case is specifically designed for metallic materials that experience a limited number of load cycles, typically less than 10,000 cycles, at high loads or stresses. The code is applicable for materials used in fusion reactors such as EUROFER97 [16]. The design fatigue curves are derived from the fit curve by applying a factor of 2 on the strain range or a factor of 20 on cycles, depending on which is more conservative at each point. The purpose of these factors is to account for various effects, such as

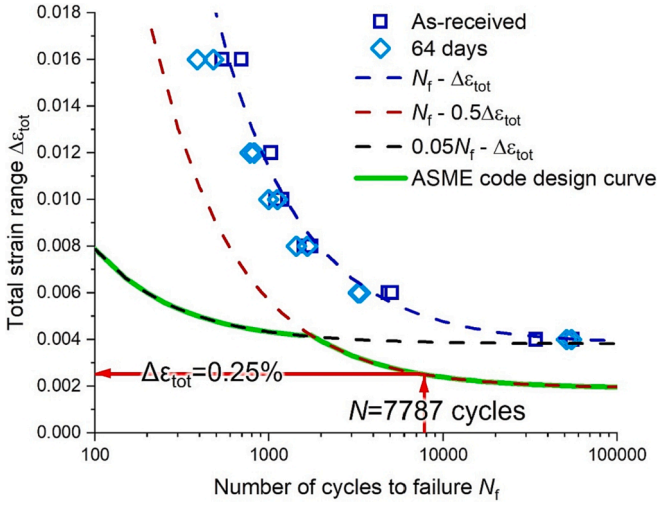

Fig. 12. Results of the LCF tests of EUROFER97 specimens in as-received and pre-corroded conditions. The N_f-$\Delta\varepsilon_{tot}$, N_f-0.5$\Delta\varepsilon_{tot}$, and 0.05N_f-$\Delta\varepsilon_{tot}$ curves are shown for the as-received specimens. The design fatigue strain range curve was built according ASME code design. The red arrows show how the allowed total strain range was determined.

environmental factors, scale differences between the material and test specimen, surface finish, and data scatter [16,17].

The obtained N_f-$0.5\Delta\varepsilon_{tot}$, and $0.05N_f$-$\Delta\varepsilon_{tot}$ curves are illustrated in Fig. 12 as red and black dashed lines, respectively. By using these two curves, the ASME design code curve was derived and is represented by the solid green line in Fig. 12. It should be noted that the data points obtained for standard specimens exposed to the ceramic breeder environment exceed the ASME design code curve. This indicates that the approach taken in this study accounts for environmental factors and surface deterioration due to pre-corrosion experiment.

To determine the number of heating and cooling cycles with tension–compression that EUROFER97 tubes inside the DEMO blanket will be subjected to, it is necessary to consider the cyclic operation of the DEMO reactor. Each DEMO cycle consists of a ramp up in 150 s, 2 h of full power operation, 150 s of ramp-down, and a 600 s dwell period [18]. Thus, a single DEMO cycle lasts for a total of 2.25 h. It is known that the first blanket in the DEMO reactor will need to operate for a duration of 2 years. Therefore, the total number of cycles N can be calculated as $N = 2{\cdot}365{\cdot}24/2.25 = 7787$ cycles. As a result, EUROFER97 tubes will be subjected to a total of 7787 heating and cooling cycles during their operational lifespan.

For a conservative estimate of the allowable total strain range, 7787 cycles can be considered the minimum number of cycles before failure, as indicated by the red arrows in Fig. 12. The maximum allowable total strain range corresponding to 7787 cycles on the ASME code design curve was then calculated to be 0.25 %. It should be emphasized that this value was determined without considering neutron irradiation and the effect of creep, which will most likely result in a further reduction of the resulting value of the allowable total strain range.

The strain induced by heating or cooling of EUROFER97 tubes (without considering the effects of creep) can be estimated and compared to the allowable total strain range limit. The strain (ε) is calculated as $\varepsilon = \alpha{\cdot}\Delta T$, with α being $11.9{\cdot}10^{-6}$ K^{-1} (within the 300–550 °C temperature range, the operational temperature for EUROFER97 tubes) and ΔT as 250 K in the same range. The calculated strain value is $\varepsilon = 0.2975\%$, slightly exceeding the allowable limit of 0.25 %. Consequently, in the case of a perfectly rigid system in constrained conditions (real conditions should be evaluated by finite element method) it is likely that the required number of cycles (7787 cycles within 2 years of operation) may not be endured by EUROFER97 tubes, even without considering the effects of strong neutron irradiation and creep.

4. Conclusions

The pre-corrosion of standard specimens in the ceramic breeder environment (exposure to the Li-ceramic pebbles in a He + 0.1vol.%H_2 purge gas atmosphere at 550 °C for 64 days) resulted in corrosion similar to that observed in the previously studied sub-sized specimens. The corrosion process led to the formation of three distinct layers with varying phase compositions, collectively measuring approximately 17 μm in thickness.

The fatigue life of standard specimens with a diameter of 8.8 mm underwent a notable reduction after pre-corrosion treatment, indicating a significant deterioration compared to the as-received specimens. Despite being subjected to the same testing conditions, the standard specimens exhibited a higher number of cycles to failure compared to the corresponding sub-sized specimens with a diameter of 2 mm. Under a strain level of 0.6 %, the exposure of the standard specimens to the ceramic breeder environment for 64 days resulted in a 35 % decrease in the fatigue life, while the sub-sized specimens experienced a more substantial reduction of 60 % under the same conditions.

A rough, corroded surface on EUROFER97 samples with imprints left by contact with lithium ceramic pebbles could be regarded as notches and lead to the accelerated formation of surface micro-cracks, even when the samples are cooled after exposure. These cracks can be considered as sites of fatigue crack initiation. Therefore, the reduction in the time required for fatigue crack initiation leads to a decrease in the total number of cycles to failure.

The maximum allowable total strain range of EUROFER97 components for 2 years of operation in DEMO (7787 cycles) was estimated using the ASME code design curve as 0.25 % without considering the effects of strong neutron irradiation and creep.

CRediT authorship contribution statement

E. Gaisina: Writing – review & editing, Methodology, Investigation, Visualization. **R. Gaisin:** Investigation, Writing – review & editing. **J. Leys:** Methodology, Writing – review & editing. **R. Knitter:** Methodology, Writing – review & editing. **J. Aktaa:** Supervision, Conceptualization, Methodology, Writing – review & editing. **M. Walter:** Supervision, Methodology, Investigation, Writing – review & editing.

Declaration of Competing Interest

The authors declare that they have no known competing financial interests or personal relationships that could have appeared to influence the work reported in this paper.

Data availability

Data will be made available on request.

Acknowledgements

The authors would like to thank Melina Blem for her assistance in mechanical testing.

This work has been partially carried out within the framework of the EUROfusion Consortium, funded by the European Union via the Euratom Research and Training Programme (Grant Agreement No 101052200 — EUROfusion). Views and opinions expressed are however those of the author(s) only and do not necessarily reflect those of the European Union or the European Commission. Neither the European Union nor the European Commission can be held responsible for them.

We acknowledge support by the KIT-Publication Fund of the Karlsruhe Institute of Technology.

References

[1] F.A. Hernández, P. Pereslavtsev, G. Zhou, B. Kiss, Q. Kang, H. Neuberger, V. Chakin, R. Gaisin, P. Vladimirov, L.V. Boccaccini, G.A. Spagnuolo, S. D'Amico, I. Moscato, Advancements in the helium-cooled pebble bed breeding blanket for the EU DEMO: Holistic design approach and lessons learned, Fusion Sci. Technol. 75 (2019) 352–364, https://doi.org/10.1080/15361055.2019.1607695.

[2] M. Gorley, G. Aiello, J. Henry, T. Nozawa, G. Pintsuk, M. Rieth, H. Tanigawa, DEMO structural materials qualification and development, Fusion Eng. Des. 170 (2021), 112513, https://doi.org/10.1016/j.fusengdes.2021.112513.

[3] R. Lindau, A. Möslang, M. Rieth, M. Klimiankou, E. Materna-Morris, A. Alamo, A.-A.-F. Tavassoli, C. Cayron, A.-M. Lancha, P. Fernandez, N. Baluc, R. Schäublin, E. Diegele, G. Filacchioni, J.W. Rensman, B. Schaaf, E. Lucon, W. Dietz, Present development status of EUROFER and ODS-EUROFER for application in blanket concepts, Fusion Eng. Des. 75–79 (2005) 989–996, https://doi.org/10.1016/j.fusengdes.2005.06.186.

[4] O. Leys, J.M. Leys, R. Knitter, Current status and future perspectives of EU ceramic breeder development, Fusion Eng. Des. 164 (2021), 112171, https://doi.org/10.1016/j.fusengdes.2020.112171.

[5] J. Aktaa, M. Walter, E. Gaisina, M. Kolb, R. Knitter, Assessment of the chemical compatibility between EUROFER and ceramic breeder with respect to fatigue lifetime, Fusion Eng. Des. 157 (2020), 111732, https://doi.org/10.1016/j.fusengdes.2020.111732.

[6] E. Gaisina, M. Duerrschnabel, J. Leys, R. Knitter, J. Aktaa, M. Walter, Recent studies to the impact of a ceramic breeder environment on the mechanical properties of EUROFER97 under operating conditions, J. Nucl. Mater. 564 (2022), 153677, https://doi.org/10.1016/j.jnucmat.2022.153677.

[7] A. E2714-13, Standard Test Method for Creep-Fatigue Testing, West Conshohocken, PA, 2013.

[8] T. Chikada, M.H. Kolb, H. Fujita, K. Nakamura, K. Kimura, M. Rasinski, Y. Hishinuma, K. Mukai, R. Knitter, Compatibility of tritium permeation barrier coatings with ceramic breeder pebbles, Corros. Sci. 182 (2021), 109288, https://doi.org/10.1016/j.corsci.2021.109288.

[9] K. Mukai, F. Sanchez, T. Hoshino, R. Knitter, Corrosion characteristics of reduced activation ferritic-martensitic steel EUROFER by Li2TiO3 with excess Li, Nuclear Materials and Energy 15 (2018) 190–194, https://doi.org/10.1016/j.nme.2018.04.010.

[10] M. Duerrschnabel, E. Gaisina, R. Gaisin, M. Walter, J. Aktaa, M. Rieth, Nanoscale insights into the corrosion of EUROFER by lithium ceramics, Corros. Sci. 199 (2022), 110190, https://doi.org/10.1016/j.corsci.2022.110190.

[11] R.G. Forman, V. Shivakumar, Growth behavior of surface cracks in the circumferential plane of solid and hollow cylinders, ASTM special technical publications (1986) 59–74.

[12] R.G. Forman, V. Shivakumar, S.R. Mettu, J.C. Newman, Jr., Fatigue Crack Growth Computer Program 'NASGRO' Version 3.00, Reference Manual: JSC-22267B, Johnson Space Center, Houston, TX, 1998.

[13] Peggy C. Miedlar, Alan P. Berens, Allan Gunderson, and J.P. Gallagher, USAF damage tolerant design handbook: Guidelines for the analysis and design of damage tolerant aircraft structures: AFRL-VA-WP-TR-2003-3002 ANALYSIS AND SUPPORT INITIATIVE FOR STRUCTURAL TECHNOLOGY (ASIST) Delivery Order 0016, Dayton, OH 45469, 2002.

[14] G. Federici, C. Bachmann, W. Biel, L. Boccaccini, F. Cismondi, S. Ciattaglia, M. Coleman, C. Day, E. Diegele, T. Franke, M. Grattarola, H. Hurzlmeier, A. Ibarra, A. Loving, F. Maviglia, B. Meszaros, C. Morlock, M. Rieth, M. Shannon, N. Taylor, M.Q. Tran, J.H. You, R. Wenninger, L. Zani, Overview of the design approach and prioritization of R&D activities towards an EU DEMO, Fusion Eng. Des. 109–111 (2016) 1464–1474, https://doi.org/10.1016/j.fusengdes.2015.11.050.

[15] G. Federici, C. Bachmann, L. Barucca, W. Biel, L. Boccaccini, R. Brown, C. Bustreo, S. Ciattaglia, F. Cismondi, M. Coleman, V. Corato, C. Day, E. Diegele, U. Fischer, T. Franke, C. Gliss, A. Ibarra, R. Kembleton, A. Loving, F. Maviglia, B. Meszaros, G. Pintsuk, N. Taylor, M.Q. Tran, C. Vorpahl, R. Wenninger, J.H. You, DEMO design activity in Europe: Progress and updates, Fusion Engineering and Design 136 (2018) 729–741, https://doi.org/10.1016/j.fusengdes.2018.04.001.

[16] J. Aktaa, M. Weick, M. Walter, High temperature creep-fatigue structural design criteria for fusion components built from EUROFER 97: Final Report: TW2-TTMS-005b, D1 TW5-TTMS-005, D7, Forschungszentrum Karlsruhe, 2007. FZKA 7309.

[17] B.F. Langer, Design of pressure vessels for low-cycle fatigue, J. Basic Eng. 84 (1962) 389–399.

[18] C. Bachmann, Plant Description Document, EUROfusion, EFDA_D_2KVWQZ. V.1.9., 2020.